

# 2D or Not 2D: A Thermodynamic Approach to Modeling Space Solar Cells' Efficiency with 2D Materials

Calista Wilk<sup>1</sup> and Peide Ye<sup>2#</sup>

<sup>1</sup>BASIS Scottsdale

<sup>2</sup>Purdue University

#Advisor

## ABSTRACT

Approximately 3 billion people have never used the internet due to its costs and inaccessibility, particularly in developing countries. To provide these areas with affordable internet, reducing the cost of building and launching satellites has become paramount in the assessment of their design, particularly their solar cells. While three-dimensional semiconductor materials like gallium arsenide (GaAs) have been the main material used in these cells to convert solar energy into electrical energy, two-dimensional (2D) materials like tellurene have demonstrated properties that warrant consideration. This research evaluates the potential of a novel 7-junction space solar cell configuration consisting of manganese phosphorus trisulfide, tungsten disulfide, rhenium disulfide, molybdenum disulfide, molybdenum ditelluride, bismuth oxyselenide, and tellurene to replace current 3-junction configurations using GaAs-based materials. Thermodynamic expressions, including the efficiency of a Carnot heat engine and a geometric optimization approach using the Shockley-Queisser triangle, were analyzed to derive equations for two properties critical to a space solar cell: efficiency and specific power. Computational simulations were run, and the results indicate that a 7-junction space solar cell configuration using 2D materials can enable a maximum efficiency gain of 12%, a mass reduction by over one-fifth, and a specific power output improvement of 54% at lower costs compared to GaAs-based space solar cells. The implications of this study point to the performance and cost feasibility of satellite usage for a broad range of applications, with social and environmental significance.

## Introduction

In recent years, satellite usage has expanded from military purposes and government-sponsored space exploration missions to commercial applications such as radio, television, and internet services. With satellites becoming increasingly critical to everyday life around the globe and consumers desiring lower prices for services, reducing the cost of building and launching satellites has become paramount in the assessment of their design, particularly their solar cells, which convert the sun's energy into electricity to power the operations on a satellite. By analyzing how novel materials can be implemented into space solar cells, this report examines ways to reduce the mass of these cells while also achieving a higher efficiency. The result is a redesigned solar cell that can potentially be integrated into satellites for improved performance at a reduced cost.

The most widely used materials in a space solar cell's absorber region, which is where incident photons are converted into electrical energy, are gallium arsenide (GaAs) and related III-V compounds. (III-V refers to materials with chemical constituents consisting of at least one element from Group III of the periodic table and at least one element from Group V, with GaAs as the most well-known example; the term III-V will be used interchangeably with

GaAs throughout the report.) III-V materials dominate this sector because these compounds have relatively high photon conversion efficiencies and high tolerance to the harsh radiation exposure in outer space.<sup>1</sup> Most current space solar cells consist of a triple junction structure, where three separate III-V absorber materials are layered on one another, such as a stack consisting of indium gallium arsenide (InGaAs), GaAs, and gallium indium phosphide (GaInP), to convert as many incident photons as possible.<sup>2</sup> However, III-V solar cells require costly, thick layers that must be deposited slowly and precisely, with compositionally graded buffers in-between, to achieve a highly ordered, high-quality crystalline film.<sup>1</sup>

An alternative approach implements two-dimensional (2D) materials, a novel and rapidly growing class of materials that are radiation tolerant,<sup>3</sup> are stable at layers a few atoms thick,<sup>4</sup> and can be deposited with atomically sharp interfaces between adjacent layers.<sup>5</sup> These 2D materials do not require thick buffer layers to transition between different materials because a defining property of this class of materials is that they form strong chemical bonds in the horizontal x-y plane but form only weak van der Waals interactions vertically between sheets of atoms. To explore the potential use of 2D materials in photovoltaic applications, one study reported a one-step growth strategy to vertically stack 2D tungsten disulfide (WS<sub>2</sub>) on top of molybdenum disulfide (MoS<sub>2</sub>),<sup>6</sup> while another successfully incorporated phosphorene nanoribbons into a perovskite solar cell to increase its efficiency.<sup>7</sup> With such promising reports, it becomes important to further investigate the capability and possible benefits of implementing 2D materials into a space solar cell to increase its efficiency and hence its performance.

A solar cell's efficiency, which is a critical factor to consider when determining how well a given cell will be able to convert photons into usable electrical energy, is strongly affected by the number of junctions it has (Fig. 1). The more junctions it has, the more photons it can absorb, and the less energy that is lost due to photons passing straight through the layer [orange and red arrows in Fig. 1(a)] or due to excess energy from an absorbed photon that is radiated away as heat [purple and blue arrows in Fig. 1(a)]. For a solar cell to reach high efficiencies, the average of the absorber layers' band gaps (the amount of energy required to excite an electron into conducting electricity) must match the average sun's photon energy of ~1.2 electron volts (eV), meaning each junction's band gap changes as the number of junctions in a cell changes.

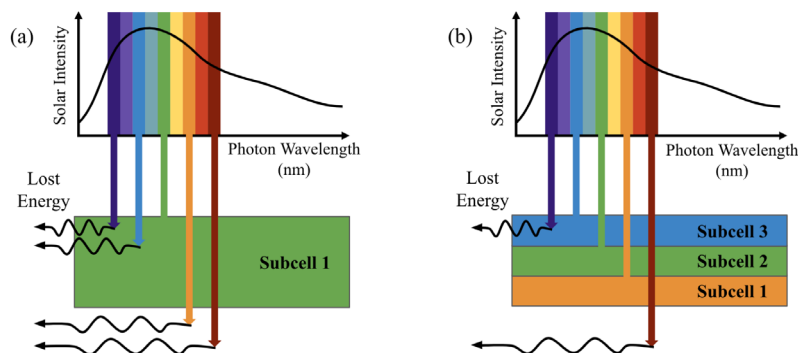


**Figure 1.** Photon wavelengths absorbed and energy lost for (a) 1-junction and (b) 3-junction cells

Therefore, the higher the number of junctions, the greater the difference is between the largest and smallest band gap values so that more of the sun's energy emission spectrum can be absorbed. This increased efficiency lowers the number of solar cell devices needed to produce a given power output, which reduces the total number of solar panels a satellite would need and leads to a significant reduction in its mass with lower associated manufacturing and launch costs.

To assess the potential of replacing GaAs-based materials with 2D materials in space solar cells, equations describing two critical parameters for performance – efficiency and specific power – were determined and evaluated to compare a 3-junction cell with 2D materials and a 7-junction cell with 2D materials against the control of a current

3-junction GaAs-based cell. By examining the results, the potential benefits of using specific 2D materials in a multi-junction configuration were analyzed, and a redesigned space solar cell was proposed to shed light on how the performance of space solar cells can be improved while reducing the cost of satellite missions. This enables satellite usage to be more accessible for a broad range of applications, with social and environmental implications.

## Methods

### Calculating Efficiency

The efficiency of a solar cell measures its ability to convert the sun's energy, in terms of emitted photons, into electrical energy in the form of electricity. This can be shown as:

$$\eta = \frac{P_{out}}{P_{in}} \tag{Eq. 1}$$

where  $\eta$  is the efficiency,  $P_{in}$  is the power input from the energy of the sun's incident photons, and  $P_{out}$  is the power output from the electricity produced.  $P_{out}$  and  $P_{in}$  are formally defined as power densities (with units of watts per square meter,  $W/m^2$ ). Since the surfaces that  $P_{out}$  is generated by and that  $P_{in}$  is incident on are part of the same solar cell and thus have the same area, the square meter units cancel out. For this reason,  $P_{out}$  and  $P_{in}$  were treated as values for power in  $W$ . Additionally, since the sun's intensity remains essentially unchanged for satellites in Earth's orbit,  $P_{in}$  was treated as a constant and equal to  $1380 W/m^2$ . Thus, maximizing the efficiency of a solar cell hinged on maximizing  $P_{out}$ . By definition of electrical power,

$$P_{max} = I_{mp}V_{mp} \tag{Eq. 2}$$

where  $P_{max}$  is the maximum power generation possible for a given solar cell,  $I_{mp}$  is the current at maximum power, and  $V_{mp}$  is the voltage at maximum power.

Through a thermodynamics approach in which a solar cell was treated as a Carnot engine,<sup>8</sup> the equations for  $I_{mp}$  and  $V_{mp}$  were determined using partial differential equations to locate the respective relative maxima of efficiency  $\eta$ , which corresponds with the maxima of  $P_{out}$ :

$$I_{mp} = q\theta_S(\gamma_S - \gamma_D)e^{-E_g/k_B T_S} \tag{Eq. 3}$$

$$V_{mp} = \frac{E_g}{q} \left(1 - \frac{T_D}{T_S}\right) - \frac{k_B T_D}{q} \ln\left(\frac{\theta_D}{\theta_S}\right) \tag{Eq. 4}$$

where  $E_g$  is the band gap of the absorber material in the solar cell, and  $q$  the charge of an electron ( $1.6 \times 10^{-19}$  Coulombs). The device temperature  $T_D$  for satellite solar cells is about 40 Kelvin (K) during operation rather than the 3 K temperature of outer space, due to a self-heating effect from electron collisions with the atomic lattice after photon capture excitation and the subsequent de-excitation.<sup>9</sup> The temperature of the sun  $T_S$  is 5777 K, and  $k_B$  is Boltzmann's constant of  $1.38 \times 10^{-23}$  Joules per Kelvin.  $\theta_D$  is the solid angle of radiation emission from the device (equal to  $2\pi$  steradians since a back plane mirror is typically used to reflect photons back onto the cell), and  $\theta_S$  is  $\sim 6.5 \times 10^{-5}$

steradians (based on the distance of the earth from the sun, the radius of the sun, and the knowledge that the sun's light rays are essentially parallel at this distance).  $\gamma$  is related to blackbody spectrum radiation and is defined as

$$\gamma_i \equiv \frac{2k_B T_i}{c^2 h^3} (E_g^2 + 2k_B T_i E_g + 2k_B^2 T_i^2) \quad \text{Eq. 5}$$

where  $c$  is the speed of light and is equal to  $3 \times 10^8$  meters per second (m/s) and  $h$  is Planck's constant of  $6.626 \times 10^{-34}$  m<sup>2</sup>kg/s. For the sun,  $\gamma_s$  has  $T_i = T_s$ , and for the solar cell device,  $\gamma_D$  has  $T_i = T_D$ . These definitions for  $\gamma_s$  and  $\gamma_D$  were used to create a more compact analytical expression for  $I_{mp}$ ; however, since  $\gamma_D$  was negligible compared to  $\gamma_s$  (as  $T_D$  was less than 1% of  $T_s$ ) in this study,  $\gamma_D$  was removed from Eq. 3. Neglecting  $\gamma_D$  introduced a small 2-3% overestimation of  $I_{mp}$  for  $E_g$  values below 1.0 eV, so an adjustment factor of 0.975 was multiplied to layers with an  $E_g$  below 1.0 eV as a minor correction.

Using the terms defined above, Eqs. 3 and 4 simplify to the following, respectively, for blackbody radiation in space (i.e., air mass zero, or AM0):

$$I_{mp} = \begin{cases} 0.975 \cdot 120(1 - 0.5E_g), & E_g < 1 \\ 44.33(4E_g^2 + 4E_g + 2)e^{-2E_g}, & E_g \geq 1 \end{cases} \quad \text{Eq. 6}$$

$$V_{mp} = 0.993 \frac{E_g}{q} - 0.0396 \quad \text{Eq. 7}$$

To obtain a compact calculable expression for  $I_{mp}$ , a minor approximation was used in the expression for incident photon flux to derive Eq. 3, such that Eq. 3 results in a slight underestimation in  $I_{mp}$  compared to Eq. 6. Therefore, Eq. 6 was used to determine efficiency since it more closely matches the formal expressions, with the exception previously mentioned of the 2-3% overestimation of  $I_{mp}$  for  $E_g < 1.0$  eV.

For the case of a single junction solar cell,  $P_{out}$  and efficiency can now be calculated based purely on the  $E_g$  value of the absorber material. However, multi-junction stacks of materials with tiered band gaps achieve higher efficiencies, so a methodology was needed to optimize values for each band gap  $E_g$ , and each  $I_{mp}$  and  $V_{mp}$ , while matching the average band gap value of the stack to the average value of photon energies emitted from the sun (~1.2 eV).

A geometric optimization approach with the Shockley-Queisser (SQ) triangle method was used to determine the ideal band gap values for any number of subcell layers stacked on one another in a cell by maximizing the area, namely the power output, under a normalized I-V curve.<sup>8</sup> Shown in Figure 2,<sup>8</sup> the total possible output power is represented by the entire triangular area underneath the red downward sloping line bounded by the x- and y-axes. Figure 2(a) is for the case of a single subcell. In Figure 2(b), the output power from each of  $N$  subcells is represented by each corresponding rectangle's area. To fill as much area of the triangle as possible, the widths of each rectangle must be equal. This equates to the current  $I_{mp}$  generated by each junction being equal, as shown by the evenly divided sections along the x-axis.

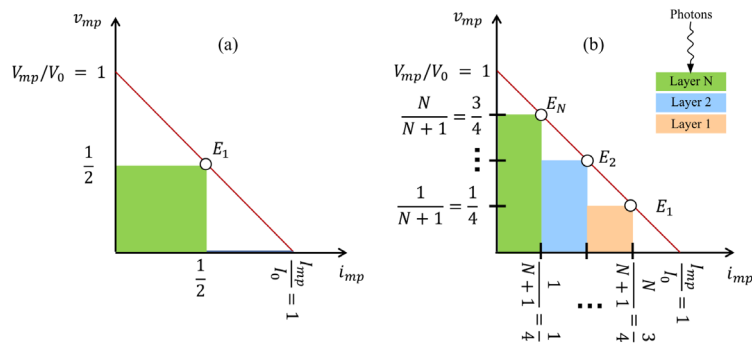


**Figure 2.** SQ triangle method to determine ideal band gap energies for maximum output power (figure taken from Alam and Khan, 2019)<sup>8</sup>

For N subcells, the equation for  $I_{mp}$  is therefore given by

$$I_{mp} = \frac{I_0}{N + 1} \tag{Eq. 8}$$

where  $I_0$  (and  $V_0$  noted below) is a normalization factor based on the sun's incident energy and the solar cell's temperature. Once  $I_{mp}$  is known,  $V_{mp}$  can be determined by the red line, which leads to the equation for the voltage at maximum power output for each layer  $i$  in the stack,

$$V_{mp,i} = \frac{iV_0}{N + 1} \tag{Eq. 9}$$

With the  $V_{mp}$  value determined for each layer in the multi-junction stack, the corresponding  $E_g$  value for each subcell can be calculated using Eq. 7.

Utilizing Eqs. 6, 7, 8, and 9, a simulator called PVLimits was programmed to calculate the optimal band gap energy for each absorber layer in a multi-junction cell as a function of the number of subcells in the device.<sup>10</sup> The input parameters for the simulations in this study were chosen for blackbody radiation from the sun (AMO) as there is no atmosphere to absorb or scatter light, and the solar cell device temperature was set at 40 K to account for self-heating,<sup>9</sup> with all other parameters set as their default values. An upper limit of nine subcells was chosen to include the highest number of junctions used in a III-V solar cell and junctions that could be redesign possibilities.<sup>11</sup> Among the 9 configurations generated, one was selected for redesign consideration, and the 3-junction configuration was highlighted to compare against a III-V 3-junction configuration. Each calculated ideal band gap value was then individually matched with a reported band gap value to identify candidate 2D materials.

With the expectation that the band gaps of the 2D materials chosen would not match the ideal band gaps exactly, the output power of the actual (non-ideal) solar cell ( $P_{out,N}$ ) was calculated for all three configurations for comparison. Based on the electrical properties of a circuit with resistors in series (the semiconductor absorber layers in a solar cell behave like resistors from a circuit perspective),  $P_{out,N}$  was calculated by adding together the  $V_{mp,i}$  value from Eq. 7 for each junction  $i$  in the cell and multiplying this sum by the minimum  $I_{mp}$  current,  $\min\{I_{mp}\}$ , produced by the entire stack of subcells. Since it is a series circuit, only one current can flow, which is equal to  $\min\{I_{mp}\}$ . Thus, the  $\min\{I_{mp}\}$  value was determined by finding the difference between the  $I_{mp}$  values from Eq. 6 for each pair of adjacent

junctions and setting  $\min\{I_{mp}\}$  equal to the smallest difference.  $P_{out,N}$ , which was calculated with the equation shown below, was substituted into Eq. 1 for  $P_{out}$  to determine the actual (non-ideal) efficiency values for each of the three multi-junction configurations:

$$P_{out,N} = \min\{I_{mp}\} \cdot \sum_{i=1}^N V_{mp,i}$$

Eq. 10

### Calculating Specific Power

After the efficiency values for each of the three configurations were determined, the specific power  $P_S$  for each structure was calculated. Specific power depends on  $P_{out}$  and the mass ( $M$ ) of the solar cell and has the equation:

$$P_S = \frac{P_{out}}{M}$$

Eq. 11

Since specific power measures how much power a solar cell can produce for its mass, maximizing specific power enables a cell to reach its highest performance level. This can be achieved by maximizing  $P_{out}$  and minimizing the solar cell's mass.  $P_{max}$  is formally defined as a power density, so to cancel out the cross-sectional area included in  $P_{max}$ , the areal mass density ( $\rho_A$ ) of the solar cell was calculated. To determine  $\rho_A$ , the areal mass density of each individual junction  $i$  ( $\rho_{A,i}$ ) and the areal mass densities of the components besides the absorber layers, such as a metal frame, electrical interconnects, and a glass casing sheet, were used. The combined areal mass density of these components for a typical 3-junction III-V solar cell is  $2.06 \text{ kg/m}^2$ .<sup>12</sup> This value was used for the solar cells with 2D materials to serve as a control variable.

For  $\rho_{A,i}$ , the thickness ( $t_i$ ) of each junction was chosen as 200 nanometers (nm) since this thickness has been shown to be sufficient to achieve values for specific power that are comparable to current III-V solar cells.<sup>13</sup> For the GaAs-based cell, the thicknesses for each junction were determined from values used in literature, with GaInP at 3 micrometers ( $\mu\text{m}$ ), GaAs at  $1 \mu\text{m}$ , and InGaAs at  $3 \mu\text{m}$ .<sup>1</sup> Each thickness value was then multiplied by the volumetric mass density ( $\rho_{V,i}$ ) of the material to determine  $\rho_{A,i}$ :

$$\rho_{A,i} = t_i \rho_{V,i}$$

Eq. 12

The absorber layers in a solar cell must also be grown on a substrate in order to provide a framework, but the thicknesses and mass densities vary depending on whether the structure is made from 2D materials or GaAs-based materials. Studies report that 2D materials can be grown on a  $5 \mu\text{m}$  polyimide substrate ( $\rho_V$  of  $1.42 \text{ g/cm}^3$ )<sup>13</sup> and that III-V triple-junction space solar cells can be grown on a  $100 \mu\text{m}$  germanium substrate ( $\rho_V$  of  $5.5 \text{ g/cm}^3$ ).<sup>14</sup> The areal mass density for each of these substrates  $\rho_{A,S}$  was calculated with Eq. 12. Summing the areal mass densities of all the junctions in a cell with the areal mass density of the substrates and other cell components gives  $\rho_A$  of the solar cell with  $N$  junctions below.

$$\rho_A = \sum_{i=1}^N \rho_{A,i} + \rho_{A,S} + 2.06$$

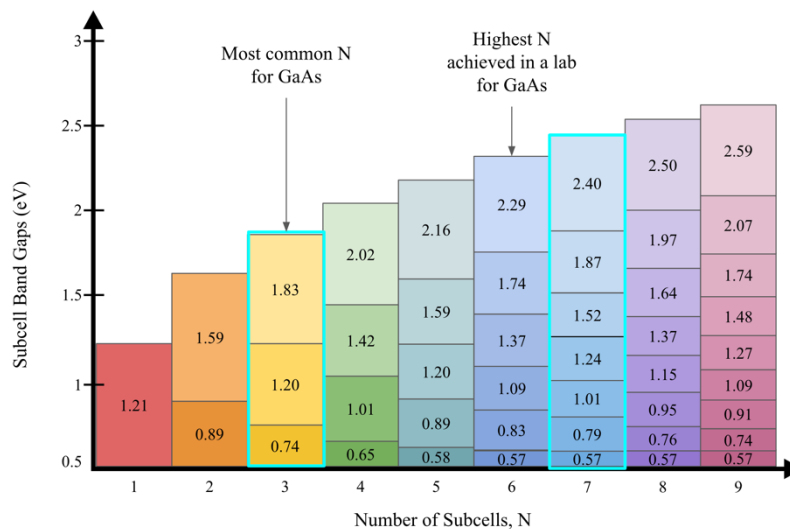
Eq. 13

The values that were calculated in Eqs. 2 and 13 were substituted into Eq. 11 to determine the maximum (ideal)

specific power for each solar cell configuration, and the values calculated in Eqs. 10 and 13 were used in Eq. 11 to determine the actual (non-ideal)  $P_s$ .

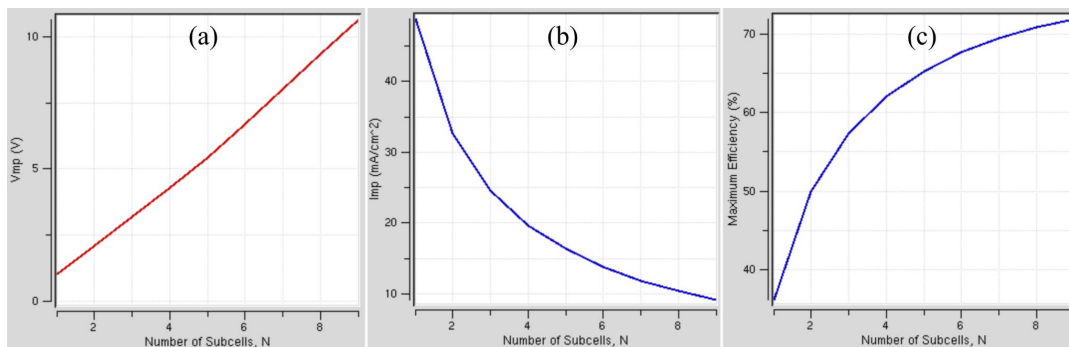
## Results

Figure 3 shows an illustration of the simulator’s output for the ideal band gap value for each subcell in a multi-junction tandem structure for up to 9 subcells. The average band gap energy of the subcell materials for all cases of N subcells is  $\sim 1.2$  eV, in accordance with the peak in photon energy from the sun’s emission spectrum in outer space. The 3-junction configuration was highlighted for comparison purposes, and the 7-junction configuration was chosen, based on the highest number of 6 junctions reported for GaAs-based cells<sup>11</sup> and the observation that the band gaps become closer in value after 7 subcells, meaning certain 2D absorber layers could become too thin to absorb enough incoming photons to be effective.



**Figure 3.** Ideal band gap for each layer in N-subcell tandem space solar cells, up to 9 subcells

The corresponding simulation results for key parameters  $V_{mp}$ ,  $I_{mp}$ , and efficiency of multi-junction tandem structures with N subcells are shown in Fig. 4. The efficiency continues to increase as N increases, shown also in Fig. 1, but the rate of increase begins to diminish for higher numbers of subcells.



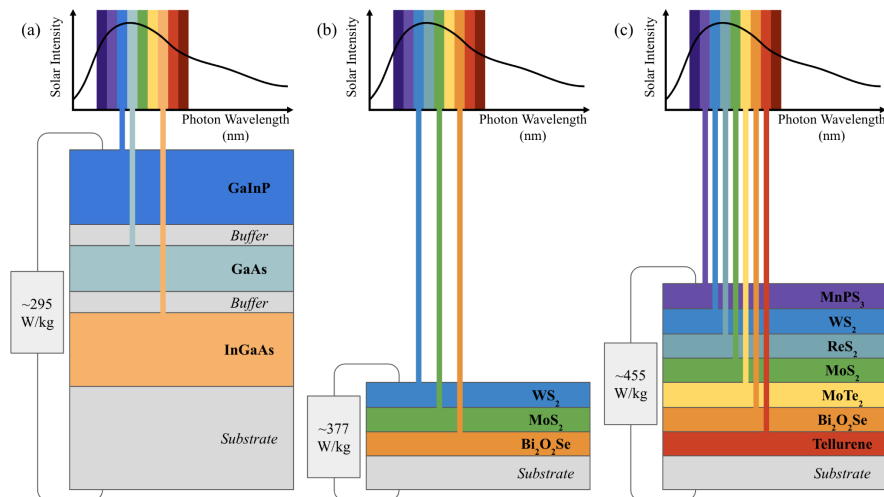
**Figure 4.** Simulation outputs for N-subcell structures for (a) voltage, (b) current, and (c) efficiency (figure produced with PVLimits)<sup>10</sup>

Table 1 shows the list of candidate 2D materials, each with their reported band gap and mass density,<sup>15-21</sup> along with reported band gaps for the III-V materials analyzed in this study.<sup>22</sup> Based on the ideal band gap values in Fig. 3, to ensure maximum absorption of photons and subsequent conversion into electrical energy, the optimal solar cell structure would arrange the materials in the order of manganese phosphorus trisulfide (MnPS<sub>3</sub>) on top, with WS<sub>2</sub>, rhenium disulfide (ReS<sub>2</sub>), MoS<sub>2</sub>, molybdenum ditelluride (MoTe<sub>2</sub>), bismuth oxyselenide (Bi<sub>2</sub>O<sub>2</sub>Se), and tellurene as the bottom layer. The 2D materials chosen for the 3-subcell structure were WS<sub>2</sub>, MoS<sub>2</sub>, and Bi<sub>2</sub>O<sub>2</sub>Se to compare with GaInP, GaAs, and InGaAs.

**Table 1.** List of reported band gaps and densities for candidate 2D and common III-V materials

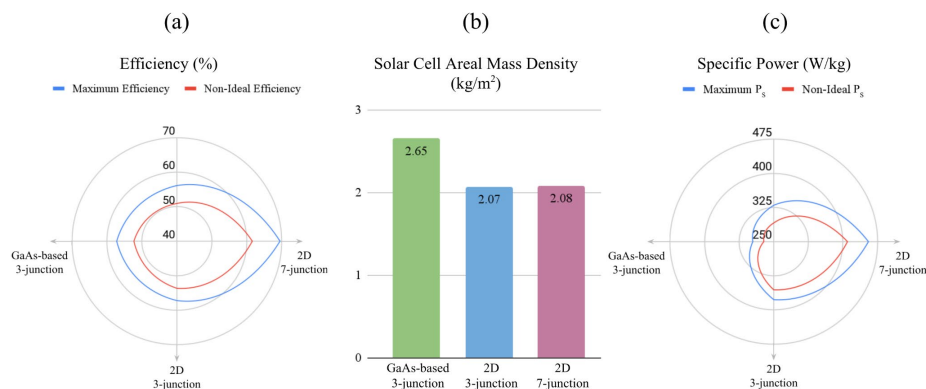
Material	Class	Band Gap Energy (eV)	Density (g/cm <sup>3</sup> )
MnPS <sub>3</sub>	2D	2.4	2.92
WS <sub>2</sub>	2D	1.9	7.50
ReS <sub>2</sub>	2D	1.5	7.60
MoS <sub>2</sub>	2D	1.2	5.06
MoTe <sub>2</sub>	2D	1.0	7.70
Bi <sub>2</sub> O <sub>2</sub> Se	2D	0.8	9.18
Tellurene	2D	0.5	6.06
GaInP	III-V	1.9	4.56
GaAs	III-V	1.4	5.32
InGaAs	III-V	0.9	5.68

Fig. 5(a) illustrates the 3-junction tandem cell of III-V materials, with Figs. 5(b) and 5(c) depicting 2D materials being used in a 3-junction and 7-junction configuration, respectively.



**Figure 5.** Illustration of stacked structures for (a) 3-junction III-V, (b) 3-junction 2D, and (c) 7-junction 2D structures

Using Eqs. 1, 10, 11, and 13 and the simulation outputs for  $V_{mp}$ ,  $I_{mp}$ , and efficiency with respect to the number of subcells (3 or 7), Fig. 6 shows how the values for maximum and actual (non-ideal) efficiency, the values for solar cell mass density, and the values for maximum and actual (non-ideal) specific power change according to the design and materials used.



**Figure 6.** Comparison of GaAs-based and 2D-material-based 3-junction and 2D-material-based 7-junction solar cells in terms of (a) maximum and actual (non-ideal) efficiencies, (b) the solar cell areal mass density, and (c) maximum and actual (non-ideal) specific power

## Discussion

Based on the results, a space solar cell with a 7-junction configuration layered, from top to bottom, with MnPS<sub>3</sub>, WS<sub>2</sub>, ReS<sub>2</sub>, MoS<sub>2</sub>, MoTe<sub>2</sub>, Bi<sub>2</sub>O<sub>2</sub>Se, and tellurene has the potential to replace current GaAs-based materials in a 3-junction configuration and has the capability to perform better than a cell with a 3-junction structure using 2D materials. With a maximum efficiency of approximately 69%, this redesigned space solar cell demonstrates a 12% increase in efficiency when compared to a current, 3-junction space solar cell with the GaAs-based materials analyzed in this study. Moreover, its specific power of ~455 W/kg is ~54% higher.

For a satellite that requires 1500 W to perform all its functions, then, the total mass of the solar cells that use this 7-subcell structure would be 3.30 kg, compared to the 5.49 kg needed by cells with the GaAs-based triple-junction configuration. Since a satellite cannot make use of excess power generation beyond its needs to operate or beyond what its batteries can store, the implementation of 2D materials in a 7-junction arrangement would enable a reduction of the number of solar cells on the satellite by 39.9%, which is a factor of nearly two-fifths. These values indicate the substantial increase in performance that is possible by using 2D materials, due to the reduction in mass which leads to an increase in specific power and efficiency.

Low-cost and comparatively fast techniques that are used to deposit 2D materials also offer manufacturers an affordable way to produce space solar cells which in turn would benefit consumers. A satellite's power system represents 20-30% of the satellite's mass and about 20% of the total satellite budget, with solar cells themselves representing approximately one-third of the power system cost.<sup>23</sup> The cost of the solar cell array, then, is about 6-7% of the total satellite cost. By eliminating the need for over one-third of the solar cell mass, a cost savings of ~2-3% of the total satellite budget could be achieved, which could amount to \$1 to \$15 million per satellite, depending on the structure used.<sup>24</sup> These cost savings illustrate the enormous potential benefit of replacing GaAs-based materials with 2D materials in space solar cells.

However, since the calculations in this paper were theoretical, the results project the potential of 2D materials, as they cannot yet be directly compared to experimentally measured efficiency and specific power values. This is primarily due to the difficulty in having a simulation account for factors that typically lower an absorber material's ability to effectively absorb photons, such as imperfections in the absorber materials' crystalline atomic lattice, defects at the interfaces between absorber layers, and non-uniformities in the layer compositions during growth. Additionally, the field of 2D materials is still growing, so there exists a need for more research to be conducted on specific properties, such as their absorption coefficients and fabrication techniques.<sup>25</sup> The pace of 2D research, though, is rapidly closing this gap, with reports showing how the efficiency of solar cells with 2D materials can increase by more than a factor

of 10 and their specific power by more than a factor of 100 in just over four years.<sup>13</sup> At this rate, the possibility of integrating 2D materials into space solar cells may not be far away.

## Conclusion

With the improvement in efficiency, the reduction in mass, and the increase in specific power that 2D materials can potentially achieve in space solar cells, this paper finds that a space solar cell with 2D materials in a 7-junction configuration is a design proposal with social and environmental implications. By replacing III-V materials with 2D materials, manufacturing costs would decrease, and more internet options could be created, one of which is affordable internet access for rural, underdeveloped, and remote areas currently unable to receive any internet services. In addition, less space debris would be generated since the lighter mass of redesigned space solar cells with 2D materials would extend the life of a satellite's power system by requiring less energy for navigation and trajectory changes. If, on the other hand, the extra solar cells made of 2D materials were to remain, they would produce more energy than a satellite would need. This excess could be converted to radiofrequency waves and then sent to Earth to provide a clean source of energy to alleviate the energy crisis of climate change by assisting countries to meet net zero carbon emissions sooner. The possibilities that open up with a space solar cell using 2D materials in a 7-junction configuration warrant a close investigation into its design since it has the potential to impact future generations in a cost-effective and efficient way.

## Acknowledgements

I would like to acknowledge Professor Peide Ye at Purdue University in the School of Electrical and Computer Engineering for his continuing support and critiques regarding the analysis and results of this research project, Professor Muhammad A. Alam at Purdue University in the School of Electrical and Computer Engineering for his time and suggestions regarding the calculations for this research project, and Ms. Natasha Proctor at BASIS Scottsdale in the Department of Physics for her inputs during the drafts of this research paper. This research was conducted from July 2021 to February 2022 at home.

## References

1. J. Li *et al.*, *Front. Phys.* **8**, 1 (2021), doi.org/10.3389/fphy.2020.631925.
2. M. W. Wanlass *et al.*, "GaInP/GaAs/GaInAs Monolithic Tandem Cells for High-Performance Solar Concentrators," *Proc. Int. Conf. on Solar Concentrators for the Generation of Electricity or Hydrogen*, Scottsdale, AZ (2005).
3. A. Krasheninnikov, *Nanoscale Horiz.* **5**, 1447 (2020), doi.org/10.1039/D0NH00465K.
4. A. Castellanos-Gomez, *Nat. Photonics* **10**, 202, doi.org/10.1038/nphoton.2016.53.
5. R. Cheng *et al.*, *Nano Lett.* **14**, 5590 (2014), doi.org/10.1021/nl502075n.
6. Y. Gong *et al.*, *Nat. Materials* **13** (12), 1135 (2014), doi.org/10.1038/nmat4091.
7. F. Gomollón-Bel, "Phosphorene nanoribbons find their first use in a solar cell just 3 years after discovery," *Chemistry World*, <https://www.chemistryworld.com/news/phosphorene-nanoribbons-find-their-first-use-in-a->

- solar-cell-just-3-years-after-discovery/4015062.article (2022).
8. M. A. Alam and M. R. Khan, Proc. Natl. Acad. Sci. U.S.A. **116** (48), 23966 (2019), doi.org/10.1073/pnas.1910745116.
  9. E. Lee and T. Luo, Sol. Energy Mater. Sol. Cells **194**, 222 (2019), doi.org/10.1016/j.solmat.2019.02.015.
  10. M. R. Khan, X. Jin, and M. A. Alam, “PVLimits: PV thermodynamic limit calculator,” nanohub.org/resources/pvlimits (2017).
  11. J. F. Geisz *et al.*, Nat. Energy **5**, 326 (2020), doi.org/10.1038/s41560-020-0598-5.
  12. Spectrolab, “Space solar panels,” www.spectrolab.com/DataSheets/Panel/panels.pdf (Accessed 27 January 2022).
  13. K. N. Nazif *et al.*, Nat. Commun. **12**, 7034 (2021), doi.org/10.1038/s41467-021-27195-7.
  14. W. Geens *et al.*, “Assessment of the Use of 100 $\mu$ m Thin Germanium Wafers for High Efficiency Space Cells,” Proc. Seventh European Space Power Conf., Stresa, Italy (2005).
  15. Z. U. Rehman *et al.*, Micromachines **9** (6), 292 (2018), doi.org/10.3390/mi9060292.
  16. T. Norden *et al.*, Nat. Commun. **10**, 4163 (2019), doi.org/10.1038/s41467-019-11966-4.
  17. M. Saeed *et al.*, Phys. B: Condens. Matter **577**, 411809 (2019), doi.org/10.1016/j.physb.2019.411809.
  18. O. V. Yazyev and A. Kis, Mater. Today **18** (1), 20 (2015), doi.org/10.1016/j.mattod.2014.07.005.
  19. C. Ruppert, O. B. Aslan, and T. F. Heinz, Nano Lett. **14** (11), 6231 (2014), doi.org/10.1021/nl502557g.
  20. C. Chen *et al.*, Science Adv. **4** (9), 1 (2018), doi.org/10.1126/sciadv.aat8355.
  21. D. K. Sang *et al.*, Nanomaterials **9** (8), 1075 (2019), doi.org/10.3390/nano9081075.
  22. S. Wojtczuk *et al.*, 35th IEEE Photovoltaic Specialists Conf., 001259 (2010), doi.org/10.1109/PVSC.2010.5614196.
  23. P. Beauchamp *et al.*, “Solar Power and Energy Storage for Planetary Missions,” NASA, www.lpi.usra.edu/opag/meetings/aug2015/presentations/day-2/11\_beauchamp.pdf (Accessed 30 January 2022).
  24. Globalcom Satellite Phones, “The cost of building and launching a satellite,” https://globalcomsatphone.com/costs/ (Accessed 1 February 2022).
  25. K. R. Paton and J. N. Coleman, Carbon **107**, 733 (2016), doi.org/10.1016/j.carbon.2016.06.043.